Localized O_2 starvation threat estimation and rapid O_2 compensation technique in air PEMFC

Saurav Mitra, Ramesh P., Siddhartha P. Duttagupta

***Abstract*—**Air breathing proton exchange membrane fuel cells (PEMFC) have now found its use in wide range of domestic and commercial energy based applications. Minimum carbon footprint, low maintenance, low heat operation, and higher energy efficiency at partial and full load conditions have made PEMFC one of the most sought after green energy sources for future. Optimization of PEMFC system parameters and its safer operation under dynamic load conditions ensure higher system output and longer device lifetime. Ensuring safety against oxygen starvation during transient load variation reduces the degradation of membrane electrode assembly (MEA). PEMFC performance optimization and safety against oxygen starvation requires efficient estimation and precise control of air supply subsystem state variables. This paper proposes a Kalman filter based estimation technique that helps estimate the fuel cell air supply subsystem performance parameters. Some parameters that are otherwise non-measurable under industrial environment are also estimated using the proposed estimation technique. The FEM based fuel cell modeling gives further insight regarding the degree of oxygen starvation in PEMFC. The qualitative membrane degradation threat occurring during oxygen starvation under fluctuating load at varying environmental humidity is also estimated here. Finally, a rapid oxygen compensation technique is proposed which helps mitigate the permanent PEMFC health damage. The proposed oxygen compensation technique ensures safe operation, longer life, higher energy efficiency, and reduced per unit energy cost obtained from the renewable energy source.

***Keywords*—**Air breathing PEMFC, Kalman filtering, membrane degradation monitoring, O_2 starvation and mitigation, transient load.

I. Introduction

PEM fuel cell is an electrochemical device that combines hydrogen and oxygen and produces electricity with heat and water as the byproducts. Production of high energy density at comparatively low temperature, high efficiency, and pollutant free quieter operation are its salient features. This nonconventional energy generation technology is uniquely suited for wide variety of industrial and vehicular applications [1]. However, ensuring safe operation of fuel cell and related subsystems under critical and dynamic load conditions is a big challenge. PEMFC shows abrupt performance and health degradation under adverse operating condition such as oxygen starvation at fluctuating sharp load transients. Maladjustment in the PEMFC subsystem inputs may cause irreversible membrane and fuel cell health damage. This paper proposes a PEMFC state estimation and control technique that ensures safe operation against oxygen starvation. The proposed rapid oxygen compensation technique inhibits and decelerates the fuel cell stack degradation and enhances its performance and lifetime.

Several researchers have so far developed different control models for air breathing PEMFC stack and related subsystems. Xue *et. a*l proposed an empirical polynomial based approximation technique [2]. Ogaji *et. al* proposed an interpolation and experimental characterization based technique to determine stack efficiency [3]. Many criteria and control strategies for overall PEMFC system control are also reported [4-5]. However, these modeling approaches are mainly based on complex system parameter interaction which do not use state space based estimation techniques [6]. Though FEM based and other fully featured 2D and 3D models precisely describe the complicated reaction phenomena within the fuel cell, they are found to be ill fitting when used with the real time digital system controllers [7].

Our work uses less computation intensive PEMFC system model. It overcomes the deficiencies of numerically exhaustive models where closed form solution of the main system variables cannot be found out easily. Our model facilitates the application of Kalman filter for non-measurable PEMFC state variable estimation. Finding the localized threat due to scarcity in oxygen supply at PEMFC cathode is quantified in this work. The results also qualitatively determine the threat of cathode air humidity variation on membrane health. Finally, an intervention technique is proposed for mitigation of irreversible oxygen starvation damage in fuel cell. This is another novelty of our work. A simpler model for the hydrogen supply subsystem is also shown here. It helps in determining state dynamics of anode fuel supply with respect to the dynamic load.

The paper is organized as follows: Section 2 describes the air supply and hydrogen supply subsystems and their combined state space models. Section 3 presents the basics of linear Kalman filtering. In section 4, the gas flow and the gas

Saurav Mitra is a Ph.D. student at the Electrical Engineering Department of Indian Institute of Technology Bombay, Mumbai -76, India. (phone: +91-22-2576-7401; fax: +91-22-2572-3707; e-mail: sauravm@ee.iitb.ac.in).

Ramesh P. is a PhD student at the Electrical Engineering Department of IIT Bombay. He is an assistant professor in the Department of Electronics and Communication Engineering at College of Engineering, County Hills, Idukki, Munnar - 685612, Kerala. (e-mail: ramp@ee.iitb.ac.in).

Siddhartha P. Duttagupta is an assistant professor with the Electrical Engineering Department of Indian Institute of Technology Bombay, Powai, Mumbai -400076, India. (e-mail: sdgupta@ee.iitb.ac.in).

Table I – Abbreviations, Symbols and Indices

CO - Air compressor pump of air supply unit
HP - Hydrogen pump of fuel supply unit
I_L - Load Current (A), $\mathbf{i_{CO}}$ - air compressor current (A)
ω - Compressor speed (rad/sec)
k_f - Friction constant of the compressor
k_t - Current build up time constant
k_m - Mechanical time constant for CO inertia build up
J - Load inertia of the compressor
V_{adm} - Input air volume at the cathode side
P_{adm} - Input air pressure at the cathode side
λ_{O2} - Oxygen Ratio
$r_{O2,a}$ - Molar mass relation between O_2 :dry air = 0.233
h - Environmental humidity ratio (0 < h < 1)
M_{am} - Inlet air molar mass (= 0.0288 Kg)
M_{O2} - Molecular mass of oxygen (= 0.032 Kg)
n - Number of single fuel cell in FC stack (= 7)
F - Faraday's constant (= 96485)
S_1 - Switch 1 and valve 1 for valve 1 control
S_2 - Switch 2 and valve 2 for valve 2 control
$\dot{m}_{air}$ - Air mass flow rate (SLPM)
$\dot{m}_{H2}$ - Hydrogen mass flow rate (SLPM)
L_{CO} - compressor motor inductor
R_{CO} - equivalent air flow resistance of the compressor and humidifier pipes
ε - porosity of the GDL layer
μ - the dynamic viscosity, (Pa.s)
ρ - the density of GDL material (Kg/m^3)
S_u - any external force term
p - reactant pressure (Pa)
u - gas velocity vector (m/s)
D_{ij}^{eff} - the effective diffusion constant
κ - the permeability (m^2)
ϕ - the phase potential
σ_m^{eff} - the effective electric conductivity (S/m)
σ_s^{eff} - the effective electrode conductivity (S/m)
S - current source term A/m^3
s - property of the solid phase
e - property of the electrolyte phase
φ_m - Volumetric fraction of ionomer in catalyst layer
T - absolute temperature in Kelvin
A - Electrode active surface area in m^2
η - Activation over-potential
R - Universal gas constant
j_0 – Exchange current density A/m^2
C_{O2} – Oxygen concentration
C_{O2}^{ref} – Reference oxygen concentration

diffusion layer mass flow modeling is explained in detail with equations. Section 5 deals with the oxygen ratio calculation and ill effects of less oxygen ratio on fuel cell health. Next, in section 6, the simulation results are presented for FEM based oxygen starvation modeling in PEMFC. Simulation results for oxygen ratio and related threat determination for fluctuating

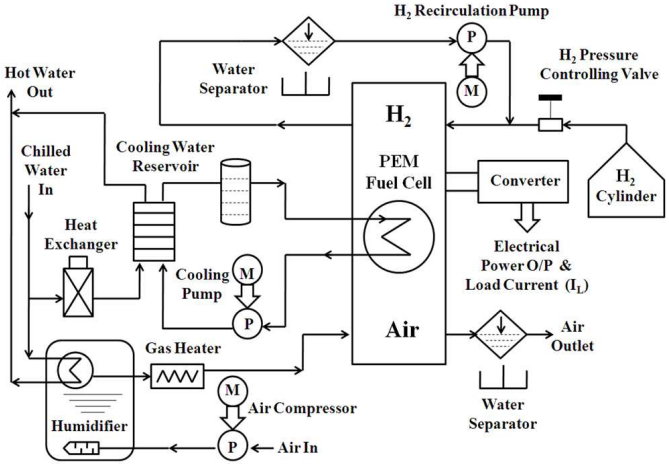

Fig. 1 PEMFC with important auxiliary subsystems

load and variable humidity are also given in section 6. The rapid oxygen compensation technique against oxygen starvation is proposed in section 7. We conclude with section 8 with mention of our future work.

II. Auxiliary System State space Model for PEMFC

PEMFC is based on solid polymer electrolyte type membrane. The basic PEMFC electrochemical reaction is given in Eq. 1. Stack voltage and I_L are the main indicators for gross efficiency and system power [8]. The physical configuration of a typical PEMFC with auxiliary subsystems

$$H_2 + \frac{1}{2}O_2 \rightarrow H_2O \,. \tag{1}$$

is shown in Fig. 1. In this case, the air supply compressor motor is not auto powered from fuel cell stack, but it is separately excited [8]. The humidity ratio of cathode air determines electrochemical reaction rate in PEMFC. Load power directly alters the $\dot{m}_{air}$ demand from air compressor [4]. ω_{CO}, i_{CO}, and I_L are directly proportional. i_{CO} and ω_{CO} are to be estimated from $\dot{m}_{air}$ sensor readings using Kalman filter.

A. Cathode Air Supply System Model

The approximated air supply system model shown in Fig. 2 is governed by the motor-compressor equations [8]. Pressure dynamics of the compressor is not considered for this particular model for simplicity. V_{CO} is compressor voltage (2).

$$V_{CO} = L_{CO}.\frac{di_{CO}}{dt} + R_{CO}.i_{CO} + k_{t,CO}.\omega_{CO}\,, \tag{2}$$

$$J_{CO}.\dot{\omega}_{CO} = k_{t,CO}.i_{CO} - k_{f,CO}.\omega_{CO}\,. \tag{3}$$

$$\dot{m}_{air} = k_{m,CO}.\omega_{CO} \tag{4}$$

B. Anode Hydrogen Supply System Model

Due to laminar flow conditions, the pressure drop at anode depends linearly on $\dot{m}_{H2}$, and ω_{HP} [8]. State of ω_{HP} is to be estimated from $\dot{m}_{H2}$ sensor readings using Kalman filter.

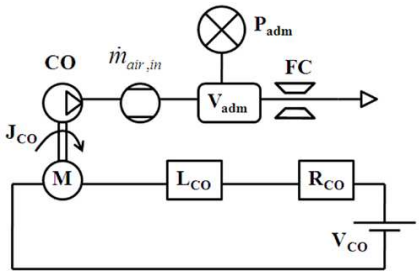

Fig. 2 Air supply subsystem Schematic with DC motor

$$J_{HP}.\dot{\omega}_{HP} = k_{t,HP}.i_{HP} - k_{f,HP}.\omega_{HP} \quad (5)$$

$$\dot{m}_{H_2} = k_{m,HP}.\omega_{HP} \quad (6)$$

C. Overall Subsystem Control Model

The state space models for the two main auxiliary systems are given in Eq. 2 to Eq. 6. They are assembled into a global state space model for the overall balance of plant model. The state and output equations for air and H_2 subsystems are modeled in a single set of state space form, Eq. 7. For the above model, air compressor voltage and anode H_2 pressure are initially adjusted by the user. Later on, the H_2 pressure is maintained by a hydro-mechanical pressure regulator [8]. This model is controllable and observable [11], [12].

$$\begin{bmatrix} \frac{di_{CO}}{dt} \\ \frac{d\omega_{CO}}{dt} \\ \frac{d\omega_{HP}}{dt} \end{bmatrix} = \begin{bmatrix} -\frac{R_{CO}}{L_{CO}} & -\frac{k_{t,CO}}{L_{CO}} & 0 \\ \frac{k_{t,CO}}{J_{CO}} & -\frac{k_{f,CO}}{J_{CO}} & 0 \\ 0 & 0 & -\frac{k_{f,HP}}{J_{HP}} \end{bmatrix} \begin{bmatrix} i_{CO} \\ \omega_{CO} \\ \omega_{HP} \end{bmatrix} + \begin{bmatrix} \frac{1}{L_{CO}} & 0 \\ 0 & 0 \\ 0 & \frac{k_{t,HP}}{J_{HP}} \end{bmatrix} \begin{bmatrix} V_{CO} \\ i_{HP} \end{bmatrix}$$

$$\begin{bmatrix} \dot{m}_{air} \\ \dot{m}_{H_2} \end{bmatrix} = \begin{bmatrix} 0 & k_{m,CO} & 0 \\ 0 & 0 & k_{m,HP} \end{bmatrix} \begin{bmatrix} i_{CO} \\ \omega_{CO} \\ \omega_{HP} \end{bmatrix} \quad (7)$$

III. KALMAN FILTER BASED SUBSYSTEM STATE ESTIMATION

To control a dynamic system, it is important to know the rate of change in system variables that is necessary to be controlled. It is not always possible within industrial environment. Kalman filter here provides a means for inferring the missing information from indirect and noisy measurements. Kalman filter is a set of mathematical equations that provides an efficient computational and recursive means to estimate the state of a process, in a way that minimizes the mean of the squared error. The filter is very powerful as it supports estimations of past, present, and even future states, and it can do so even when the precise nature of the modeled system is unknown [9]. It is the best linear unbiased estimator. For Kalman filter (KF) based dynamic system state estimation, it is assumed that the system is perturbed by white noise and the measurements that are linearly related to the states are also corrupted by white noise [10], [14]. A time varying linear stochastic differential equation as a model of a random process has the general form

$$x(t) = F(t)x(t) + G(t)w(t) + C(t)u(t), \quad (8)$$

$$z(t) = H(t)x(t) + v(t) + D(t)u(t). \quad (9)$$

The values of x(t) in the differential equation model over time define vector valued Markov process. This model is the representation for many real world processes; including stationary and nonstationary Gaussian processes [10]. KF implementation in discrete time domain requires discrete time random sequence of the process. Vector valued discrete time recursive equation for random sequence model is given as

$$x_k = \Phi_{k-1}x_{k-1} + G_{k-1}w_{k-1} + \Gamma_{k-1}u_{k-1}, \quad (10)$$

$$z_k = H_k x_k + v_k + D_k u_k, \quad (11)$$

here x_k is state vector, z_k is measurement vector, u_k is deterministic control input vector, Φ_{k-1} is dynamic coefficient matrix, G_{k-1} is process noise coupling matrix, Γ_{k-1} is input coupling matrix, H_k is measurement sensitive matrix, D_k is output coupling matrix, w_k is zero mean uncorrelated process noise, and v_k is zero mean uncorrelated measurement noise [10]. The expected values are:

$E[w_k]=E[v_k]=0$,
$E[w_{k1}.w_{k2}^T]=Q_{k1}.\Delta(k_2-k_1)$; (Kronecker Delta)
$E[v_{k1}.v_{k2}^T]=R_{k1}.\Delta(k_2-k_1)$,
$E[w_{k1}.v_{k2}^T]=M_{k1}.\Delta(k_2-k_1)$.

Discrete Kalman Filter Equations

In this formulation of the discrete Kalman filter, G matrix has been combined with the plant noise covariance [10].

System dynamic model: $x_k = \Phi_{k-1}x_{k-1} + w_{k-1} + \Gamma_{k-1}u_{k-1}$, where $w_k \sim N(0, Q_k)$.

Measurement model: $z_k = H_k x_k + v_k$, $v_k \sim N(0, R_k)$.

Initial conditions: $E[x_0] = \hat{x}_0$, and $E[\tilde{x}_0\tilde{x}_0^T] = P_0$.

Independence assumption: $E[w_k.v_j^T] = 0$, for all k & j

State estimate extrapolation:

$$\hat{x}_k(-) = \Phi_{k-1}\hat{x}_{k-1}(+) + \Gamma_{k-1}u_{k-1}.$$

Error covariance extrapolation: (12)

$$P_k(-) = \Phi_{k-1}P_{k-1}(+)\Phi_{k-1}^T + Q_{k-1}.$$

Kalman gain matrix: $\bar{K}_k = Pk(-)H_k^T[H_kP_k(-)H_k^T + R_k]^{-1}$.

State estimate observational update:

$$\hat{x}_k(+) = \hat{x}_k(-) + \bar{K}_k[z_k - H_k\hat{x}_k(-)].$$

Error covariance update: $P_k(+) = [I - \bar{K}_kH_k]P_k(-)$. [10]

Kalman filter is implemented for state vector propagation where simulated or real measurements data are available. Covariance matrix positive semi definiteness and controllability and observability of the initial state space formulation are necessarily to be checked for the success of Kalman filter based estimation.

IV. Flow Channel and Gas Diffusion Layer Mass Flow Modeling In PEMFC

Degradation in fuel cell performance is one of the main challenges for developing a commercial fuel cell system for automotive applications. Oxygen starvation at reaction sites is a major issue in air fed fuel cell systems under varying atmospheric conditions. Degradation is mainly caused by undesired side reactions such as carbon corrosion and water electrolysis under oxygen starvation conditions [15]. A drop of the electrolyte potential is observed in the oxygen starved regions of the cell. As a result, the difference between the electric potential of the cathode and the ionic potential of the electrolyte increases resulting in significant carbon corrosion and water electrolysis reaction rates [15], [16]. The described phenomenon causing severe and irreversible cell degradation is known as the reverse current decay mechanism in literature [15]. It is important to understand the mathematical models for the reactant flow channel and gas diffusion layer for better understanding of oxygen starvation process in PEMFC [13].

A. PEMFC Flow Channel Model

According to the mass conservation or continuity equation, the change of mass in a unit volume must be equal to the sum of all species entering or exiting the volume in a given time period. This law applies to the flow field plates, gas diffusion layer (GDL), and the catalyst layer. Momentum conservation relates net rate of change of momentum per unit volume due to convection, pressure, viscous friction and pore structure. This law applies to the flow field plates, GDL and the catalyst layer. The gas flow within the channel is assumed to take place by convection and diffusion [17], [18] .The gas flow in the gas channel is modeled with the momentum conservation equation and with the continuity equation -

$$\frac{\partial(\varepsilon\rho u)}{\partial t}+\nabla.(\varepsilon\rho uu)=-\varepsilon\Delta p+\nabla.(\varepsilon\mu^{eff}\Delta u)+S_u \quad (13)$$

$$\frac{\partial(\rho\varepsilon)}{\partial t}+\nabla.(\varepsilon\rho u)=0. \quad (14)$$

These equations together are called the Navier-Stokes equations. These equations are applied in the gas channel with source term equal to zero. Same equation is accounted as Darcy's law in the GDL and catalyst layer to describe the flow in the porous media. The flow occurs along with the viscous effects that are important at the boundary between the flow channel and the GDL. Species conservation relates the net rate of species mass change due to convection, diffusion and electrochemical reaction. The most commonly used equation is the Stefan-Maxwell diffusion equation (15). Charge conservation here corresponds to the continuity of current in a conducting material. This is applied to the GDL and the membrane. The mass flux in the gas phase is also based on the Maxwell-Stefan diffusion and convection equations. For a species j, the equation is described as

$$\nabla.(\rho X_i u)=\nabla.(\rho\sum_{j=1}^{n-1}D_{ij}^{eff}\nabla X_j)+S_i, \quad (15)$$

where the effective binary diffusion coefficients takes into account the porosity and tortuosity of the porous media using effective media theory.

B. PEMFC Gas Diffusion Layer and Catalyst Layer Model

Since gas diffusion layers and catalyst layers are porous media, the velocity distribution is therefore formulated by Darcy's law and mass conservation equation.

$$u=-\frac{\kappa}{\mu}\nabla P \ . \quad (16)$$

The continuity of current in a conducting material is given by

$$\nabla.i=0 \ . \quad (17)$$

In a PEM fuel cell, the conducting materials are porous electrodes and membrane. The current therefore splits into two parts: the ionic current and the electronic current. Protons travel through the ionic conductor (the membrane) to form an ionic current denoted by i_e, while electrons can only be transferred through the solid matrix of electrodes which results in an electronic current denoted by i_s. The continuity equation of current then becomes

$$\nabla.i=\nabla.i_s+\nabla.i_e 0 \ . \quad (18)$$

In the catalyst layer, where a chemical reaction occurs on a three-phase boundary, electrons are either transferred from the solid matrix to electrolyte or vice versa. This two-way transfer of electrons between solid matrix and electrolyte makes the transfer current density, denoted by j, a source term in one phase, and a sink term in the other phase. The potential equations for both solid and electrolyte phases are obtained by applying Ohm's law to Eq. (24).

Electron transport equation

$$\nabla.(\sigma_s^{eff}\nabla\phi_s)+S_{\phi s}=0 \quad (19)$$

Proton transport equation

$$\nabla.(\sigma_m^{eff}\nabla\phi_m)+S_{\phi e}=0 \quad (20)$$

The source terms in the electron and proton transport equations, i.e., Eq. (25-26), result from the electrochemical reaction occurring in the catalyst layers of anode and cathode sides. The effective conductivity σ_m^{eff} is given by

$$\sigma_m^{eff}=\varphi_m^{1.5}e^{1268\left(\frac{1}{303}-\frac{1}{T}\right)}.(0.5139\lambda-0.326) \text{ for } \lambda>1 \quad (21)$$

and $\sigma_m^{eff}=\varphi_m^{1.5}e^{1268\left(\frac{1}{303}-\frac{1}{T}\right)}(0.1879) \text{ for } \lambda\le 1$,

where λ is the water content in the membrane phase which is related to the activity of water vapor in the adjacent pores given by $a=\chi_{H2O}\frac{P}{P_{sat}}$.

Here P is the gas pressure, P_{sat} is the saturation gas pressure, χ_{H2O} is the gas phase water mass fraction. Using an experimentally derived relationship by Springer for Nafion 117 membrane

$$\lambda = 0.043 + 17.81a - 39.85a^2 + 36a^3 \text{ for } 0 \le a \le 1 \quad (22)$$
and $\lambda = 14 + 1.4(a-1)$ for $a > 1$.

The source terms are anode catalyst layer and cathode catalyst layer

$$S_{\phi s} = -j_a S_{\phi s} = -j_c \quad (23)$$

$$S_{\phi e} = j_a S_{\phi s} = j_c \quad (24)$$

Where j_a and j_c are the transfer current density corresponding to the electrochemical reaction at the anode and cathode catalyst layers [19], [20]. The transfer current densities are given by Butler-Volmer equations

$$j_a = A j_{0,a}^{ref} \left(\frac{C_{H2}}{C_{H2}^{ref}} \right) \left(e^{-\alpha_{c,a} \eta_a F/RT} - e^{\alpha_{a,a} \eta_a F/RT} \right) \quad (25)$$

$$j_c = A j_{0,c}^{ref} \left(\frac{C_{O2}}{C_{O2}^{ref}} \right) \left(e^{-\alpha_{c,c} \eta_a F/RT} - e^{\alpha_{a,c} \eta_a F/RT} \right) \quad (26)$$

The present model is established based on the following assumptions:

1. Flow is laminar everywhere due to small gas pressure gradient.
2. Reactant gases behave as the ideal gas mixture.
3. The electrodes and membrane are made of homogeneous materials.
4. The temperature distribution across the cell is uniform.
5. Water exists only in the gas phase in the fuel cell.
6. The polymer electrolyte membrane is impermeable to reactant gases.
7. Only protons can get transported through the electrolyte, and electrons through the load.
8. Three species including oxygen, water and nitrogen are considered on the cathode side while only hydrogen and water are considered on the anode side.
9. The fuel cell is operating at the steady state.

V. Oxygen Starvation and Oxygen Ratio Determination in PEMFC

The stoichiometric relation between hydrogen and oxygen supplied to the fuel cell stack and the cathode air flow mass needs to be controlled to achieve maximum stack efficiency and to avoid oxygen starvation in PEMFC. At the same time, the parasitic losses at the compressors are also to be minimized [5]. When the oxygen partial pressure falls below a critical level within meandering path of the cathode air stream, the possibility of oxygen starvation occurs [5]. During the transient load change, the phenomenon can be so severe that it might cause hot-spot or even burn-through the electrolyte surface [5]. This irreversible membrane damage causes sharp decrease in power output and reduction in PEMFC life [15]. A continuous cathode air supply monitoring process either has to remove the load or trigger system shutdown to avert permanent fuel cell membrane damage. Hence, for the safe fuel cell operation and longevity, oxygen ratio regulation becomes highly important. The oxygen ratio is given by λ_{O2} which is -

λ_{O_2} = oxygen at cathode / oxygen needed for reaction

or

$$\lambda_{O_2} = \frac{r_{O_2,a} \cdot \frac{1}{1+h} \cdot \frac{M_{am}}{(22.4).(60)} . \dot{m}_{air}}{M_{O_2} \cdot \frac{n.I_L}{4F}} . \quad (27)$$

Theoretically the value of λ_{O2} should be greater than 1 for safe PEMFC operation. A safety factor of 2 or more is considered for practical operational safety at certain load condition [15]. Environmental parameter h and system parameter I_L and $\dot{m}_{air}$ affect λ_{O2} [8]. $\dot{m}_{air}$ and $\dot{m}_{H2}$ readings of mass flow sensors are used to estimate i_{CO}, ω_{CO}, and ω_{HP} states. As $\dot{m}_{air}$ and ω_{CO} are linearly related, dynamic behavior of noise free air mass flow can be found from output equations of (7). Same process gives noise free $\dot{m}_{H2}$ from estimated ω_{HP} and linear relation between and ω_{HP} and, $\dot{m}_{H2}$ (7). For time varying I_L and corresponding air mass flow rate characteristics, λ_{O2} are calculated for different environmental humidity ratio over the entire operational period. The time instances and corresponding i_{CO} values are identified when the λ_{O2} values fall below the safety margin of 2. These are the points when intervention criterion is applied to stop further reduction in λ_{O2} value and to ensure PEMFC safety. The whole process is explained in detail in section VI.B with the help of graphs.

VI. Results

Simulations have been performed here for two cases. In the first case, a 3D PEMFC model has been created for FEM analysis with oxygen starvation. The polarization curves and electrolyte potentials are found out during oxygen starvation at different humidity conditions. In the second case, oxygen starvation threat has been found out for the PEMFC model of (7). Eq. 27 is used to find the oxygen ratio. Though the first case and the second case use different mathematical models, but the findings in both these cases are complementary to each other as they both gives threat estimation information related to O_2 starvation in fuel cell channel and related degradation in fuel cell membrane and output variable.

A. Oxygen Starvation Analysis in FEM Model of PEMFC

A three dimensional model of a PEM fuel cell is implemented using COMSOL Multiphysics platform. The schematic of the model is shown in Fig. 3. The membrane electrode assembly (MEA) is sandwiched between the cathode and the anode electrode with the polymer electrolyte kept in between. The following are some of the specifications and operating conditions used during the COMSOL modeling

- Fuel cell channel length (L) = 20 mm
- Channel height = 1 mm
- Channel width = 0.7mm
- Rib width = 1 mm
- GDL width = 0.3 mm
- Porous electrode thickness = 0.5 mm
- Membrane thickness = 0.05 mm
- GDL Porosity = 0.4

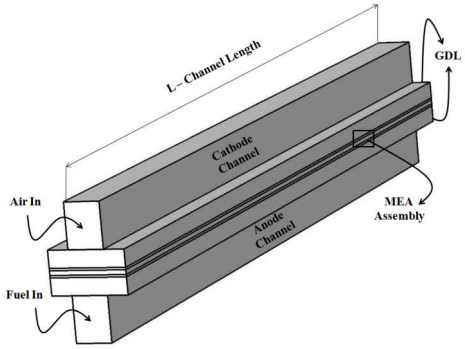

Fig. 3 Schematic of simulated fuel cell structure

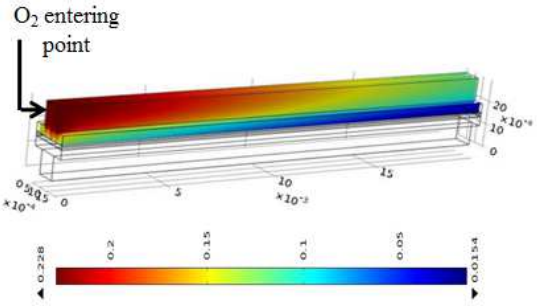

Fig. 4(a) Low O_2 starvation, humidity 25%

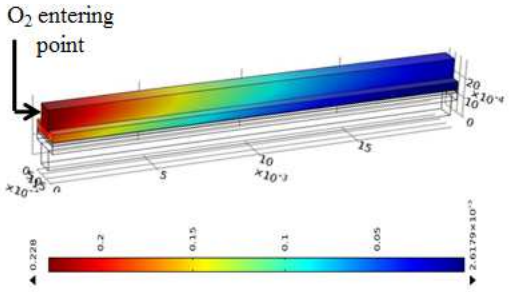

Fig. 4(b) Half channel O_2 starvation, humidity 50%

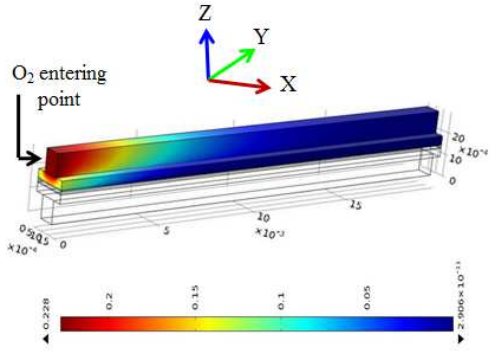

Fig. 4(c) Severe O_2 starvation, humidity 100%

- GDL electric conductivity = 1000 S/m
- Inlet H_2 mass fraction (anode) = 0.743
- Inlet H_2O mass fraction (cathode) = 0.023
- Inlet O_2 mass fraction (cathode) = 0.228
- Anode inlet flow velocity = 0.2m/s
- Cathode inlet flow velocity = 0.5m/s
- Permeability (porous electrode) = 2.36E-12 m^2
- Membrane conductivity = 10 S/m

Increment in humidity, carbon dioxide concentration and other contaminants cause reduction in oxygen content in the cathode air supply. This is a general cause for fuel cell oxygen starvation [15]. But, a sharp incremental load transient might also cause oxygen starvation in fuel cell cathode. During sharp load transients, the rate of electrochemical reaction increases rapidly. If due to system inertia, the air supply subsystem is unable to fulfill the transient air / oxygen demand at the cathode side, oxygen starvation takes place at fuel cell cathode [15]. The cathode air humidity is stepwise increased to study the consequent oxygen starvation and fuel cell degradation mechanism. Here, three conditions are simulated and their effects on fuel cell performance are analyzed. In the first case, an atmospheric relative humidity of 25% is considered. The relative humidity is increased to 50% and 100% in second and third case respectively. For all these three cases, the fuel cell membrane is initially assumed to be optimally hydrated. The electrolyte potential variation along the fuel cell channel, the polarization curves and the surface oxygen concentration variations are also studied for all these three cases. In the first case, the effect of oxygen starvation is found to be least or negligible as cathode air humidity is less. In second case, O_2 starvation occurs starting from half of the channel till the end

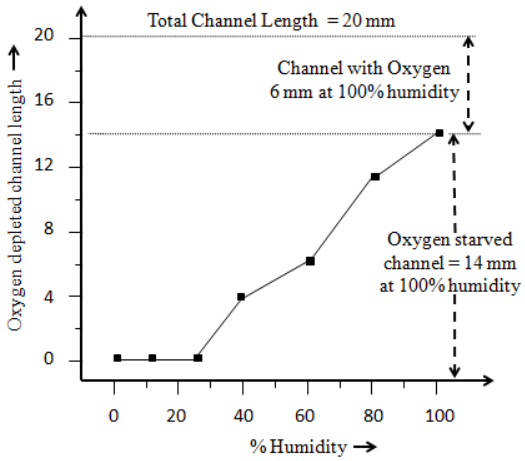

Fig. 5 Humidity vs. Oxygen depleted FC channel length

or towards the oxygen exit point. In the third case, the oxygen starvation occurs almost in the entire channel from the beginning of the channel. The channel oxygen concentrations in all these three cases are shown in Fig. 4(a, b, and c). Fig. 5 shows the oxygen starved channel length as per increment in cathode air humidity ratio. The variation in electrolyte potential along the channel and the polarization curves are shown for all three different humidity ratios in Fig. 6 and Fig. 7 respectively. The maximum power densities in all three cases are also found from the polarization curves, Fig 7(a, b and c).

Simulation results show the effects of different degrees of oxygen starvation on fuel cell output and health. It is found that the fuel cell electrolyte potential drops when the O_2 concentration falls locally. It happens due to significant carbon corrosion reaction rate in O_2 starved regions of the electrolyte

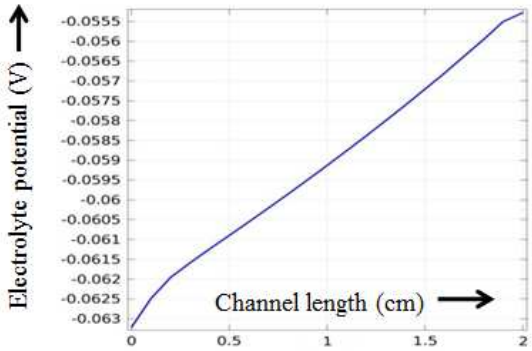

Fig. 6(a) Relative humidity 25%

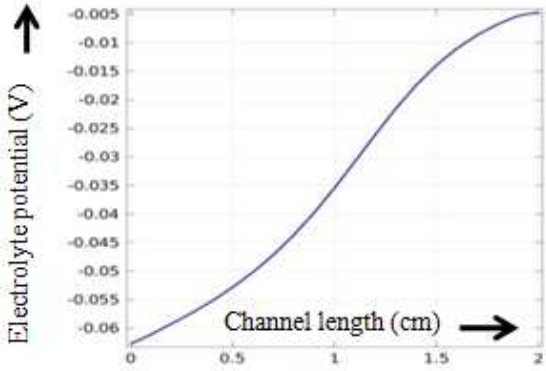

Fig. 6(b) Relative humidity 50%

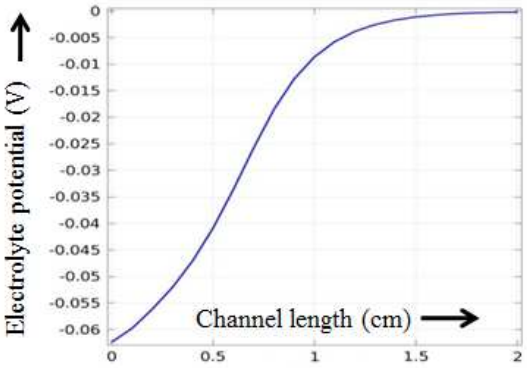

Fig. 6(c) Relative humidity 100%

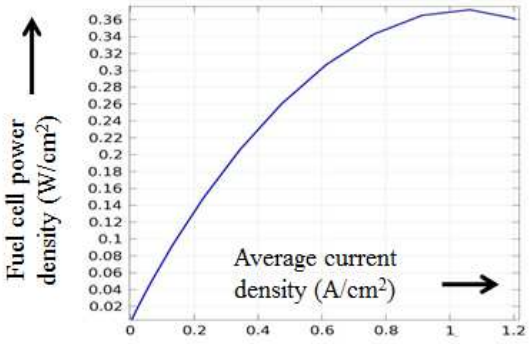

Fig. 7(a) Polarization for relative humidity 25%

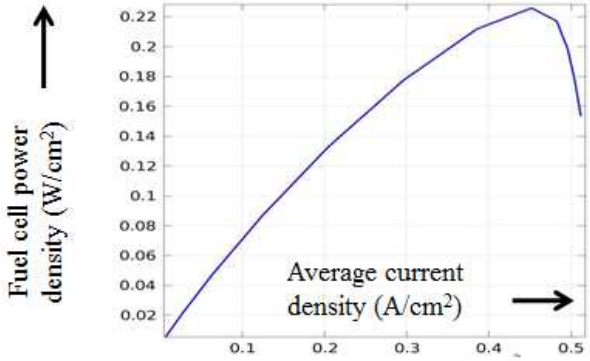

Fig. 7(b) Polarization for relative humidity 50%

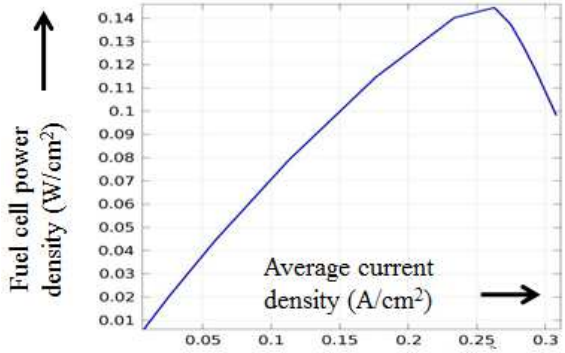

Fig. 7(c) Polarization for relative humidity 100%

This is in accordance with the reverse current decay mechanism [16]. With 25% humidity, negligible or very low O_2 starvation occurs along the channel as the channel remains fully O_2 rich. This fact is very well understood from the O_2 concentration plot given in Fig. 4(a). Figure 6(a) shows highly linear variation in electrolyte potential from -0.063 V to -0.055 V along the channel. In this close to optimal situation, the drop in electrolyte potential is not significant to cause any carbon corrosion. Hence there are no severe performance drop or degradation issues observed in the first case. Figure 7(a) gives the polarization curve for the fuel cell under the first case. The peak power density of 370 mW/cm^2 is obtained at 1.06 A/Cm^2 fuel cell average current density. In the second case, the relative humidity level of cathode air is increased to 50% which decreases O_2 concentration in the cathode air supply.

This creates higher non-uniformity in O_2 concentration along the reaction boundaries. Fig. 4(b) shows that the O_2 concentration drops to large extent from 15 mm onwards till the end of the channel end length of 20 mm. The lowest O_2 concentration in Fig 4(a) was 0.0154 mol/m^3 at the extreme right end of the channel. This O_2 concentration is good enough to run fuel cell normally. But in the second case, Fig. 4(b), oxygen concentration found in the right side end of the cathode channel (L=20 mm) is 2.6179E-3. This O_2 concentration indicates O_2 starvation in the channel. Fig. 6(b) shows higher nonlinearity in electrolyte potential variation along the fuel cell channel. This figure shows that the electrolyte potential goes to -0.01 V and more from channel length of 16 mm where the O_2 concentration has dropped considerably. Hence it is possible that heavy carbon corrosion

may occur in the channel length ranging from 16mm to 20mm. From Fig. 7(b) it is found that the maximum power density drops to 230 mW per square centimeter for this second case of operation. This power density is 140 units less than that observed in the first case. Finally, the results for maximum (100%) O_2 starvation is plotted in Fig. 4(c), 6(c), and 7(c). Fig. 4(c) shows the O_2 concentration plot along the channel and it is observed that from channel length of 6 mm onwards, O_2 concentration drops to a drastically low value unsuitable for normal fuel cell operation. The electrolyte potential drops close to zero from channel length 6 mm onwards which can be observed from Fig.4(c). From channel length 10mm onwards, the electrolyte potential goes to -0.01 V or more. This leaves very narrow linear operating region for the fuel cell at this O_2 starved condition. So the cell is completely devoid of O_2 from channel length 14 mm onwards. Significant carbon corrosion will occur in this region causing irreversible membrane degradation and considerable drop in fuel cell output power, Fig.6(c). Maximum fuel cell power density is found out to be only 150 mW/cm^2, Fig. 7(c). This is significantly less than maximum power obtained in the first case, Fig. 7(a). The irreversible carbon corrosion effectively reduces the reaction area of the fuel cell electrode. This causes fuel cell performance drop and also reduces fuel cell operating life.

B. Oxygen Starvation Ratio Based PEMFC Threat Analysis

Simulations have been performed using MATLAB 7.9 version. The fuel cell stack BRESCA FC is considered for this work. The stack is liquid cooled and provides average 65 Watts from each of 7 PEM fuel cells [8]. Operating temperature is 70^{o}C, air and hydrogen stoichiometry is 2. Operating fuel pressure is 2 bar atmosphere. Membrane surface area of each cell is 200 cm^2 [8]. The air compressor that supplies the stack is ASF Thomas 2907CDC22, a double head membrane compressor. The DC motor that supplies this compressor requires 12V DC input voltage. Maximum air flow rate from this compressor is 63 SLPM at a relative pressure of 1 bar. A KNF N 828 KNDC type single head membrane pump

$$\begin{bmatrix} \frac{di_{CO}}{dt} \\ \frac{d\omega_{CO}}{dt} \\ \frac{d\omega_{HP}}{dt} \end{bmatrix} = \begin{bmatrix} -2.89 & -1.53 & 0 \\ 150 & -15.2 & 0 \\ 0 & 0 & -1.99 \end{bmatrix} \begin{bmatrix} i_{CO} \\ \omega_{CO} \\ \omega_{HP} \end{bmatrix} + \begin{bmatrix} 35.3 & 0 \\ 0 & 0 \\ 0 & 227 \end{bmatrix} \begin{bmatrix} V_{CO} \\ i_{HP} \end{bmatrix}$$

$$\begin{bmatrix} \dot{m}_{air} \\ \dot{m}_{H_2} \end{bmatrix} = \begin{bmatrix} 0 & 0.284 & 0 \\ 0 & 0 & 0.132 \end{bmatrix} \begin{bmatrix} i_{CO} \\ \omega_{CO} \\ \omega_{HP} \end{bmatrix} \quad (28)$$

supplies the hydrogen to the fuel cell. At the design point of 0.3 bar, the H_2 flow rate is approximately 20 SLPM [8]. The overall air supply and H_2 supply subsystem model of Eq. 7 is validated and the values are shown in Eq. 28. V_{CO} is considered to be 12 V and i_{HP} is 2 A [8].

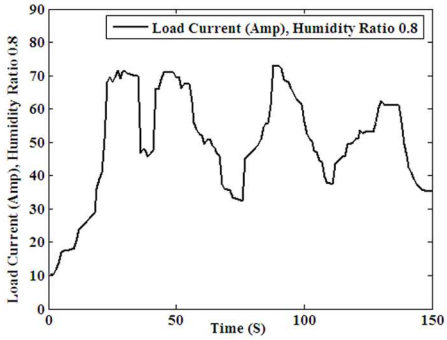

Fig. 8 PEMFC load profile at h = 0.8

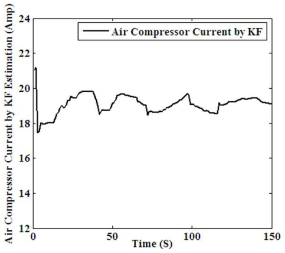

Fig. 9 KF estimated i_{CO} for load profile of Fig. 8

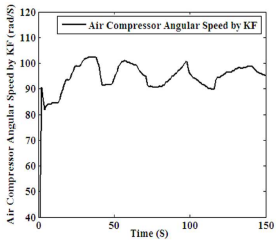

Fig. 10 KF estimated ω_{CO} for load profile of Fig. 8

The process of load profiling is carried out for different humidity ratios. Fig. 8 shows PEMFC load profile at h=0.8. From the system specifications and system model, $\dot{m}_{air}$ and $\dot{m}_{H2}$ measurement data are generated (28). KF estimation is carried out next to determine i_{CO} and ω_{CO} profiles. Fig. 9 and Fig. 10 show these profiles at h = 0.8. Next, profile for noise free $\dot{m}_{air}$ is generated from linear relation between $\dot{m}_{air}$ and ω_{CO}, Fig. 11. The whole process of load profiling, mass air flow measurements and state estimation is carried out also for h=0.4. Fig. 12 and Fig. 13 show the gradual decrement in O_2 ratio for the humidity ratio 0.4, and 0.8 respectively. These also account for the incremental threat on fuel cell membrane degradation and health damage. Fig. 12 shows that throughout the operational period, λ_{O2} is above the safety threshold of 2. It means, at lesser h of value 0.4, no irreversible health damage occurs to the fuel cell. O_2 supplied by the air supply unit is sufficient for the chemical reaction at h=0.4. It is understandable that 0.4 is lot less of a humidity ratio for optimal fuel cell output. Hence for this value of h, electrochemical reaction rate is lesser. Fig. 13 shows severity of the health damage related threat at h=0.8. Three regions R_1, R_2 and R_3 are found with λ_{O2} value less than 2. As the humidity value increases, rate of chemical reaction also increases in a non-linear fashion. Because of higher inertia, the air flow supply unit cannot meet up this nonlinear demand. Hence the probability of localized hotspot generation increases during higher load transients at higher humidity value. The O_2 rich special compressed air storage must be triggered on at the starting points of region R_1, R_2, and R_3 to avert irreversible device health damage. An alert signal is generated by the criticality monitoring unit as soon as λ_{O2} starts to fall below the value of 2 and starts going towards the value of 1, Fig. 13.

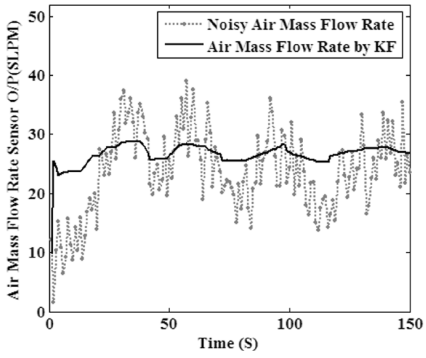

Fig. 11 Noisy and noise free $\dot{m}_{air}$ sensor reading

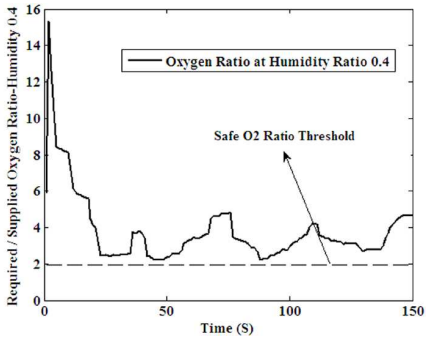

Fig. 12 Estimated Oxygen ratio at h = 0.4, no degradation threat

VII. Rapid Oxygen Compensation for Mitigation of Oxygen Starvation Threat in PEMFC

After the brief explanation of cause and effects of localized oxygen starvation in previous sections, a smart controller based oxygen compensation technique is proposed in this section. In general practice, PEMFC is used for the rated load condition. Whereas, the transient load compensation is done by means of batteries or ultra-capacitors. These techniques mainly solve the problem of inadequate hydrogen fuel supply at the anode side of PEM cell at transients. The rapid oxygen compensation technique proposed here mainly addresses the inadequacy of air supply at the cathode during transient conditions, Fig. 14. It is proposed to connect a cylinder of compressed oxygen rich air at cathode. Oxygen and nitrogen percentage within this cylinder is kept to be 25 % and 75% respectively. Other environmental gases like carbon dioxide, argon, and contaminants like carbon monoxide are absent within this special storage. Humidity within this oxygen rich storage is kept to be zero. It serves two purposes – i) compressed oxygen rich air flow at cathode suffices the higher oxygen demand during peak chemical reaction rate at cathode in transient conditions and ii) humidity free cathode air supply increases the λ_{O2} ratio instantly and prevents the danger of localized membrane damage. It shows instant performance improvement at FC power output. The storage is kept off during rated load operation and turned on only when the λ_{O2} starts falling below the safety margin of 2 and heads toward the λ_{O2} danger region of 1 - regions R_1, R_2 and R_3, Fig. 13. Respective i_{CO} values at those instants act as the trigger signal

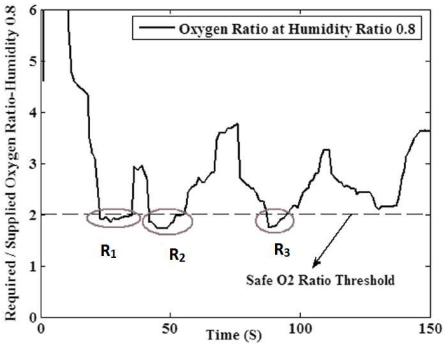

Fig. 13 Estimated Oxygen ratio at h = 0.8, severe threat

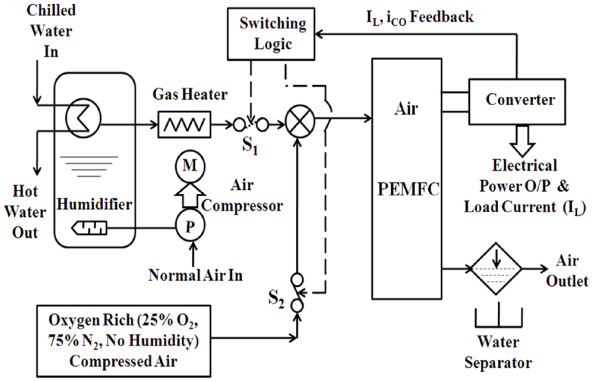

Fig. 14 Intelligent switching control for rapid O_2 compensation for PEMFC safety against O_2 starvation

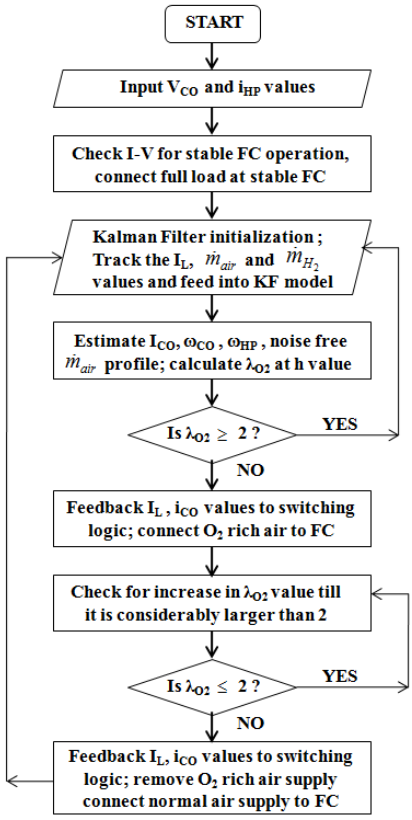

Fig. 15 λ_{O2} finding and O_2 compenstion flow chart

that closes the valve 1 of environmental air flow in and opens up the valve 2 of the special compressed air storage, Fig. 14. The microcontroller controlled switch 1 and switch 2 for valve 1 and 2 respectively operate in mutually exclusive mode, Fig. 14. When the fuel cell comes out from the transient load condition to the rated load, I_L reduces, and consequently i_{CO} reduces. This triggers the valve 1 to open and valve 2 to close, and special storage ceases to supply the FC. This is a novel compensation technique useful for ensuring longer life of the energy source with limited added system cost. The process flow is shown in Fig. 15.

VIII. Conclusion

In this work, first the state space control model for PEM fuel cell is explained with air supply and hydrogen supply auxiliary subsystems. Variations in system states are estimated next for dynamic load using Kalman filter. A qualitative analysis is obtained next for the sufficiency of supplied cathode O_2 during higher rate of chemical reaction or load transients. Finally a fuel cell membrane damage threat has been estimated from the O_2 starvation point of view at transient load. An intelligent logic controller based intervention criterion is proposed. The switching logic alters the air flow path from normal air to an O_2 rich, zero humidity ratio source. It helps in rapid compensation of localized O_2 starvation at membrane and averts irreversible membrane damage. Accelerated testing for degradation analysis of fuel cell and operating life enhancement of fuel cell with this rapid O_2 compensation technique is a part of our future research.

Acknowledgment

We express our sincere thanks to Crompton Greaves India Limited, Mumbai for sponsoring the research work.

References

[1] Saurav Mitra, P. Ramesh, B. Mitun, Duttagupta SP., "Multimode sensing technique for carbon monoxide plume tracking and forecasting for reliable field deployed air breathing PEM fuel cell operation," *Proceedings of IEEE Symposium, ISPTS 1*, Pune, India, March 2012, pp. 98-101.

[2] Xue X., Cheng K., and Sutanto D., "Unified mathematical modeling of steady state and dynamic voltage-current characteristics for PEM fuel cells," *Electrochemical Acta*, vol. 52, no. 3, 2006, pp. 1135-1144.

[3] Ogaji S. Singh R., Pilidis P., and Diacakis M., "Modeling fuel cell performance using artificial intelligence," *Journal of Power Sources*, vol.154, no. 1, 2006, pp. 192-197.

[4] Ramos-Paja C.A., Bordons C., Romero A., and Martinez Salamero L. "Minimum fuel consumption strategy for PEM fuel cells," *IEEE Transactions on Industrial Electronics*, vol. 56, no. 3, pp. March 2009, 685-696.

[5] Pukrushpan J.T., Stefanopoulou A.G., and Peng H., "Control of fuel cell breathing," *IEEE Control Systems Magazine*, vol. 24, issue 2, April 2004, pp. 30-46.

[6] Rios R., Ramos C., and Espinosa J., "Nonlinear state space model and control strategy for PEM fuel cell systems," *Journal SCIELO Colombia, Dyna*, Nr 166, Medellin, April 2011, pp. 60-67.

[7] Grasser E., and Rufer A.C., "An analytical control-oriented state space model for a PEM fuel cell system," *Proceedings of IEEE* Power Converter Conference, Nagoya, Japan, 2007, pp. 441-447.

[8] Grasser F., *An analytical control-oriented state space model for a PEM fuel cell system*. PhD thesis, Ecole Polytechnique, Lausanne, 2005.

[9] Greg Welch, and Gary Bishop, *An Introduction to Kalman Filter*, UNC-Chapel Hill,TR 95-041, July 24, 2006. http://www.cs.unc.edu/~welch

[10] Grewal M.S., and Andrews A.P., *Kalman Filtering – Theory and Practice Using MATLAB*, 3rd ed., Wiley, 2008, pp. 67-115.

[11] N. Vordos, D. V. Bandekas, J. W. Nolan, J. G. Fantidis, and A. Ioannou, "Design and simulation of hybrid power system with wind turbines, photovoltaics and fuel cells," *In Proceedings, WSEAS 1st International Conference on Power Engineering, Energy, and Electrical Drives*, PEED 2013, Cambridge, Massachusetts, USA, January 2013, pp. 19- 24.

[12] Jaroslaw Milewski, and Janusz Lewandowski, "Mathematical modeling of a molten carbonate fuel cell for CO_2 separation," *In Proceedings, WSEAS 6th International Conference on Renewable Energy Sources*, RES 12, Porto, Portugal, July 2012, pp. 122-127.

[13] Mohamed Gabbasa, and Kamaruzzaman Sopian, "Review of the electrodes layer for unitized regenerative proton exchange membrane fuel cells," *In Proceedings, WSEAS 1st International Conference on Energy and Environment Technologies and Equipment*, EEETE 12, Zlin, Czech Republic, September 2012, pp. 163-168.

[14] Noratzi Sansui, Azami Zaharim, and Kamaruzzaman Sopian, "An initial review: stochastic application in wind speed forecasting," *In Proceedings, WSEAS 1st International Conference on Power Engineering, Energy, and Electrical Drives*, PEED 2013, Cambridge, Massachusetts, USA, January 2013, pp. 82-86.

[15] Saurav Mitra, , Ramesh P., and S. P. Duttagupta, "Threat estimation of localized O_2 starvation in air breathing PEMFC and rapid O_2 compensation by intelligent control technique," *In Proceedings, WSEAS 1st International Conference on Power Engineering, Energy, and Electrical Drives*, PEED 2013, Cambridge, Massachusetts, USA, January 2013, pp. 49-54.

[16] C. A. Reiser, L. Bregoli, T.W. Patterson, J.S. Yi, J.D. Yang, M.L. Perry, and T.D. Jarvi, "A reverse current decay mechanism for fuel cells," *Electrochemical and Solid-State Letters* 8, (2005) pp. A273–A276.

[17] Adrew Rowe, and Xianguo Li. "Mathematical modelling of proton exchange membrane fuel cells." *Journal of Power Sources*, 2001, pp. 82-96.

[18] S Dutta, S. Shimpalee, and J W Van Zee. "Three Dimensional numerical simulation of straight channel PEM Fuel Cells." *Journal of Applied Electrochemistry*, 2000, pp. 135-146.

[19] Sukkee Um, C Y Wang, and K S Chen. "Computational fluid dynamics modelling of proton exchange membrane fuel cells." *Journal of the Electrochemical Society*, 2000, pp. 4485-4493.

[20] Vladimir Gurau, Hongtan Liu, and Sadik Kakac. "Two dimensional model for proton exchange membrane fuel cells." *AIChE Journal*, 1998, pp. 2410-2422.

Saurav Mitra, born in Basirhat, West Bengal, India on February 19th 1978, received Bachelor in Engineering degree in electronics from TKIET, Warananagar, Shivaji University, Maharashtra, India in 1999. He received M-Tech degree in instrumentation engineering from SGGSIET, SRTM University, Maharashtra, India in 2006. Since January 2009, he is pursuing Ph. D. in electrical engineering department in Indian Institute of Technology Bombay, Mumbai.

He was an assistant professor in the department of electronics and telecommunication engineering in RMCET, Ratnagiri, Mumbai University, India till December 2008. He has publications in twelve international journals and conferences. His research interests include fuel cell performance optimization, fuel cell control and degradation analysis, sensor networks based event source localization, digital signal processing, statistical signal processing, and power optimization from renewable energy sources.

Prof. Mitra is a life member of The Indian Society for Technical Education ISTE). He was the university gold medalist in electronics engineering in Shivaji University in 1999.

Ramesh. P was born in Trivandrum, Kerala, India in the year 1977. He obtained his undergraduate degree in the year 2000 from Cochin University of Science and Technology in Electronics Engineering as specialization. In 2003, he obtained his post graduate degree in Instrumentation Engineering from Kerala University. Currently he is pursuing his Ph. D. from electrical engineering department of IIT Bombay in the field of fabrication, modeling and testing of micro fuel cells.

He joined College of Engineering Munnar, Kerala, India in the year 2004. There he is working till date as an assistant professor in the Department of Electronics and Communication Engineering. He has international and national conference publications in the field of fuel cells. He is actively involved in research and development activities in his current institution.

Mr Ramesh is an active IEEE member for the past 16 years and has held various positions in IEEE India council.Also he is a member of Indian Society for Technical Education and Institute of Engineers India.

Siddhartha P. Duttagupta obtained his B.Tech. (Honours) from the Indian Institute of Technology, Kharagpur, India in 1991 and the Ph.D. from the University of Rochester, Rochester, New York, USA in 1998.

He was a faculty member at Boise State University, Boise, Idaho, USA from 1997-2002, and at the Indian Institute of Technology, Bombay, Mumbai, India from 2002 onwards, where he is currently an Assistant Professor. While being deeply involved in academics, he was also associated with the private sector, primarily in the cutting-edge sectors of renewable energy and nanotechnology.

Dr. Duttagupta has research interests in the area of micro-system design and micro / nano process optimization. Currently his research contribution can be measured in terms of a significant citation impact (> 1000) and an H-index of 12. He has published and presented over 100 papers in these areas, and acted as a referee for leading international journals. He also has been awarded two Indian patents and has authored two books. Dr. Duttagupta has been involved with multiple sponsored projects from agencies based in India and in the USA in the capacity of principal and co-investigator.